Fluorescent and electrochemical dual-mode detection of Chikungunya virus E1 protein using fluorophore-embedded and redox probe-encapsulated liposomes

Fluorescent and electrochemical dual-mode detection of Chikungunya virus E1 protein using fluorophore-embedded and redox probe-encapsulated liposomes

Fahmida Nasrin[1,#] · Ankan Dutta Chowdhury[2,#] · Akhilesh Babu Ganganboina[2] · Ojodomo J. Achadu[2] · Farzana Hossain[3] · Masahito Yamazaki[3] · Enoch Y. Park[*,1,2]

[1]Laboratory of Biotechnology, Graduate School of Science and Technology, Shizuoka University, 836 Ohya, Suruga-ku, Shizuoka 422-8529, Japan

[2] Laboratory of Biotechnology, Research Institute of Green Science and Technology, Shizuoka University, 836 Ohya, Suruga-ku, Shizuoka 422-8529, Japan

[3] Research Institute of Electronics, Shizuoka University, 836 Ohya, Suruga-ku, Shizuoka 422-8529, Japan

E-mail

* Enoch Y. Park
park.enoch@shizuoka.ac.jp
Fahmida Nasrin
fahmida.nasrin.17@shizuoka.ac.jp
Ankan Dutta Chowdhury
ankan.dutta.chowdhury@shizuoka.ac.jp
Akhilesh Babu Ganganboina
akhilesh.babu.ganganboina@shizuoka.ac.jp
Ojodomo J. Achadu
ojodomo.john.achadu@shizuoka.ac.jp
Farzana Hossain
farzana.hossain.17@shizuoka.ac.jp (FH)
Masahito Yamazaki
yamazaki.masahito@shizuoka.ac.jp (MY)

[*]Corresponding author at: Research Institute of Green Science and Technology, Shizuoka University, 836 Ohya, Suruga-ku, Shizuoka 422-8529, Japan.
E-mail address: park.enoch@shizuoka.ac.jp (E.Y. Park). Tel (Fax): +81-54-238-4887)

[#]these authors contribute equally

Abstract

The critical goal of sensitive virus detection should apply in the early stage of infection, which may increase the probable survival rate. To achieve the low detection limit for the early stage where a small number of viruses are present in the sample, proper amplified signals from a sensor can make readable and reliable detection. In this work, a new model of fluorescent and electrochemical dual-mode detection system has been developed to detect virus, taking recombinant Chikungunya virus E1 protein (CHIK-VP) as an example. The hydrophobic quantum dots (QDs) embedded in the lipid bilayer of liposome and methylene blue (MB) encapsulated in the inner core of liposomes played a role of dual-signaling modulator. After the CHIK-VP addition, the nanocomposites and APTES-coated Fe_3O_4 nanoparticles (Fe_3O_4 NPs) conjugated with antibodies to form a sandwich structure and separated from the medium magnetically. The nanoconjugates have been burst out by chloroform as surfactant, and both the QDs and MB are released from the liposome and then monitored the changes through fluorescence and electrochemical signals, respectively. These two fluorometric and electrochemical signals alteration quantified the CHIK-VP in the range of femto to nanogram mL^{-1} level with a LOD of 32 fg mL^{-1}, making this liposomal system as a potential matrix in virus detection platform.

Keywords: Liposomes · Quantum dots · Biosensor · Chikungunya virus protein · Fluorescence · Electrochemical

Introduction

Virus detection with higher sensitivity and selectivity, along with the presence of other interferences, is of great importance to control the annual epidemic [1–5]. In most viral diseases, the progress of vaccination is a time-consuming process that encourages the necessity for the development of rapid sensing technologies to prevent the viral outbreak. The rapid identification and quantification of viruses in all possible samples are of great significance for prompt treatment and effective management of illness [6–8]. Conventional virus detection methods like polymerase chain reaction (PCR) and other branched-chain DNA-based methodologies are not well-suited for point-of-care diagnosis [9,10]. These are time-consuming, expensive, and require intensive sample preparation with high skilled personnel [11–13]. Therefore, the development of an alternative method of virus detection is in high demand, detecting the viruses in its early stage of infection with high sensitivity and performing in real-time monitoring purposes.

Target amplification is employed using the liposomal matrix to attain high sensitivity, which has emerged in the last decade as an attractive approach where a target virus bound to a single liposome can generate amplified signals by releasing the encapsulated signal probes [14–17]. Therefore, a small number of viruses can generate an intense signal from the liposome's encapsulated probes [18–21]. Moreover, the encapsulated signal probes can be protected inside the liposome until the external triggers appear and significantly reduce the background noise, which is the great advantage of using liposome-based systems. However, in a real-time application, to attain the detectability of the virus at a very low concentration in the sample medium where a lot of impurities can interfere with the sensing, it is essential to purify the target virus from its medium. To achieve this, the well-established Fe_3O_4 magnetic nanoparticles can be extremely useful for removing the interferences from the virus-loaded

liposomal platform after proper modification [22–29]. The magnetic nanoparticles' application is quite common in recent literature due to its facile synthesis, APTES modification, and the high magnetic moment [26,30,31]. Though there are some advantages of encapsulated probes in the liposomal matrix for amplification of signals, however, from previous reports, it can be noted that the reliability of the detection remains questionable, especially in low concentration range [26, 31]. Therefore, a successful combination of the liposomal matrix with magnetic nanoparticles can be applied to construct a new class of the biosensor where multiple detections can strengthen the results.

Energized by few recent reports on liposomal amplification and magnetic separation, in this study, a dual functional signal amplification system containing fluorescent quantum dots (QDs) embedded and methylene blue-encapsulated liposomes (QDs-liposome@MB) have been synthesized for the detection of Chikungunya virus E1 protein (CHIK-VP). Recombinant CHIK-VP has been taken here as an example to establish the sensing methodology. This new class of nanocomposite, containing fluorescent and an electrochemical sensing probe, can provide double responsive sensing of a single analyte to enhance the system's reliability over other liposome-based platforms. In addition to different concentrations of CHIK-VP, the specific antibody-conjugated QDs-liposome@MB and Fe_3O_4 nanoparticles can bind with the CHIK-VP, and it can make a sandwich structure, as pictured in **Scheme 1**. The whole conjugates (QDs-liposome@MB with CHIK-VP-Fe_3O_4) have been separated magnetically from the medium to discard the interferences and excess liposomes. A surfactant can then disrupt the liposomal formation and release the fluorophores and redox probes for analysis. Hence, several probes can come out from the conjugates in the presence of a few numbers of CHIK-VP, and the detection signal can be amplified in both processes of fluorescence and electrochemical differential pulse voltammetry (DPV), respectively. In combination with the magnetic separation and dual-mode detection, here, it can be expected to establish a new

sensing mechanism where dual signals from a single analyte make more reliable testing results for real sample analysis.

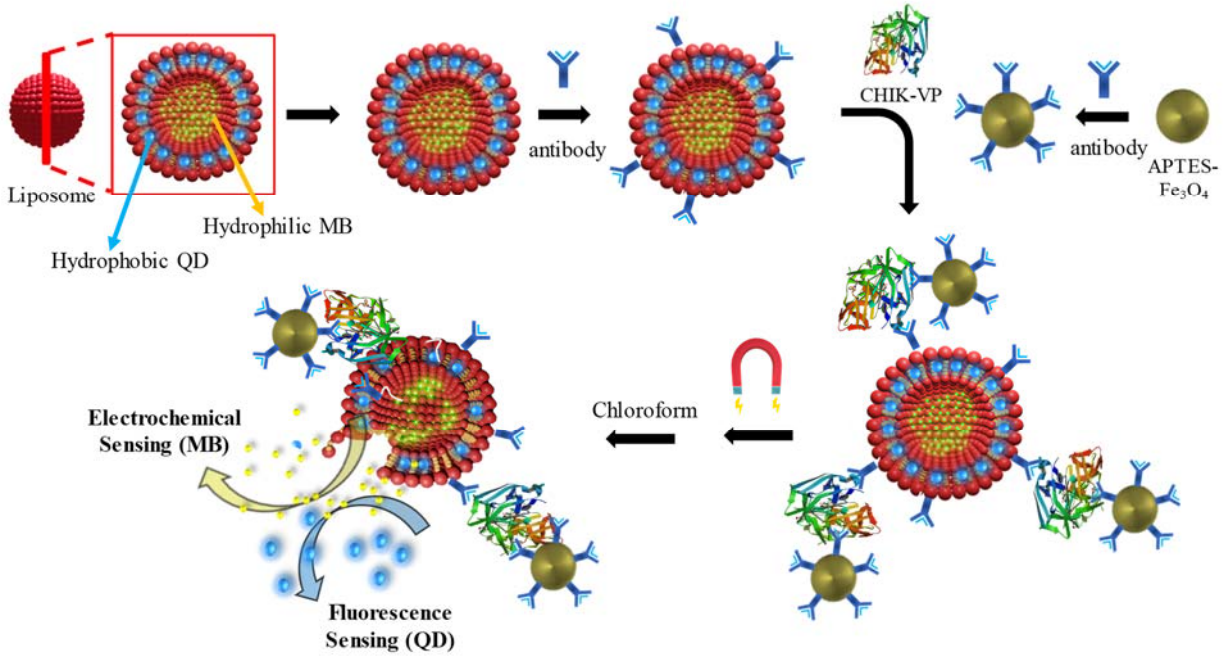

Scheme 1. Schematic representation of the formation of QDs-liposome@MB and its sandwich hybridization with Fe_3O_4 nanoparticles and its dual-mode detection mechanism for CHIK-VP detection.

Materials and methods

Chemicals and biological materials

Dry toluene, 1-octadecene, cadmium oxide (CdO), Selenium (Se), hexadecylamine (HAD), trioctylphosphine oxide (TOPO), trioctylphosphine (TOP), (3-aminopropyl)-triethoxysilane (APTES), N-hydroxy succinimide (NHS), N-(3-(dimethylamino)-propyl)-N′-ethylcarbodiimide hydrochloride (EDC) and methylene blue were purchased from Sigma-Aldrich (St Louis, MO, USA). 1-Palmitoyl-2-oleoyl-sn-glycero-3-phosphocholine (DOPC), 1,2-distearoyl-sn-glycero-3-phosphoethanolamine-N-[amino(polyethylene glycol)-2000]

111 (ammonium salt) (DSPE-PEG_{2000} amine), and 1,2-dioleoyl-sn-glycero-3-phospho-(1'-rac-
112 glycerol) (DOPG) were acquired from Avanti polar lipids (Alabaster, AL, USA). 28% (w/v)
113 ammonia solution is obtained from Duksan Pure Chemical Co., Ltd. (Ansan-si, South Korea).
114 Phosphate-buffered saline (PBS), $FeCl_2 \cdot 4H_2O$, $FeCl_3 \cdot 6H_2O$, methanol, chloroform, acetone,
115 and sodium citrate were purchased from Wako Pure Chemical Industries Ltd. (Japan).
116 Recombinant chikungunya virus E1 protein [ab 187240] and anti-chikungunya virus
117 antibody [B 1413M] [ab 130889] were purchased from Abcam Inc. (Cambridge, UK). For
118 conducting selectivity test, white-spot syndrome virus (WSSV), hepatitis E virus-like particles
119 (HEV-LP), zika virus, and influenza virus A (H3N2) were kindly provided by Dr. Jun Satoh,
120 National Research Institute of Aquaculture of Japan Fisheries Research and Education Agency,
121 Dr. Tian-Cheng Li of National Institute of Infectious Diseases, Japan, Professor K. Morita of
122 Institute of Tropical Medicine Nagasaki University, and Dr. C. Kawakami of the Yokohama
123 City Institute of Health (Yokohama Japan), respectively.
124

125 **Apparatus**

126 Dynamic light scattering (DLS) measurements were performed using a Zetasizer Nano series
127 (Malvern Inst. Ltd., Malvern, UK). A confocal laser scanning microscope (FV-1000, Olympus,
128 Tokyo, Japan) was used to take the liposome image using a stage thermocontrol system
129 (Thermoplate, Tokai Hit, Shizuoka, Japan). Fluorescence spectra and UV–vis absorption was
130 taken by using a microplate reader (Infinite F500; TECAN, Ltd, Männedorf, Switzerland).
131 Transmission electron microscopy (TEM) images of QDs, Fe_3O_4, liposomes, and their
132 nanocomposites were obtained by JEOL TEM (JEOL, Tokyo, Japan). Electrochemical DPV
133 was performed by an SP-150 (BioLogic.inc, Tokyo, Japan) in a saturated Ag/AgCl, with a
134 conventional three-electrode cell consisting of a glassy carbon disk electrode (4 mm in

135 diameter) as the counter, reference, and working electrodes, respectively (EC frontier, Tokyo,
136 Japan).
137

138 **Preparation of CdSe QDs**

139 Necessary precursors such as CdO, ODE, HDA, TOP, Se, and OA were used to perform the
140 organometallic hot-injection synthesis of hydrophobic CdSe QDs followed by a previously
141 reported procedure [32].
142

143 **Synthesis of APTES-coated Fe_3O_4 nanoparticles**

144 The synthesis of magnetic Fe_3O_4 nanoparticle was followed by a previously reported standard
145 method [33,34]. As-synthesized magnetic Fe_3O_4 nanoparticles were coated with APTES by
146 previously reported salinization method. To dissolve the APTES, dry toluene was used as the
147 reaction medium, and finally, the as-synthesized Fe_3O_4 nanoparticles were added into the
148 solution. To obtain the APTES-coated Fe_3O_4 nanoparticles, the mixture of the solution was
149 refluxed at 120°C for 20 h with continuous stirring. Finally, the APTES-coated Fe_3O_4
150 nanoparticles were rinsed with fresh toluene to remove the remaining APTES and were dried
151 overnight and stored.
152

153 **Preparation of CdSe QDs-embedded and methylene blue (MB)-encapsulated**
154 **liposome**

155 The as-synthesized hydrophobic CdSe QDs were centrifuged for 10 min at 11,000 ×g and then
156 re-dispersed in chloroform to measure the concentration. MB solutions were prepared by
157 dilution method from its stock solution of 10 mM in PBS.

158 Twenty μL of hydrophobic CdSe QDs dissolved in chloroform and 200 μL of 10 mM
159 phospholipid mixtures solution of DOPC: DOPG: DSPE-PEG_{2000} (molar ratio 50:40:10) in

160 chloroform were added into 5-mL glass vials and was evaporated by a flow of nitrogen gas to
161 produce a thin homogeneous lipid film layer on the glass wall [22]. Then the vial was stored in
162 a vacuum desiccator for 12 h to evaporate completely. The fluorescence image of lipid film
163 containing QDs is given in Fig. S1, ESM. To make the homogeneous lipid suspension, 1 mL
164 of the MB solution (various concentrations as mentioned later) was used to hydrate the lipid
165 film and agitated on a vortex mixer until the lipid film was entirely detached from the glass
166 walls. The process of forming the liposome has schematically presented in Fig. S2. Finally, the
167 lipid suspension was dialyzed using a 2 kDa dialysis bag for 24 h to get purified unilamellar
168 monodisperse QDs-liposome@MB by membrane filtering method.
169

170 **Antibody conjugation on QDs-liposome@MB and Fe_3O_4 nanoparticles**

171 The anti-CHIK-VP antibody was conjugated to the amine-functionalized liposome and
172 APTES-coated Fe_3O_4 nanoparticles separately, according to the previously reported protocols
173 [35–37]. Initially, the carboxyl group of antibodies was activated using EDC/NHS. After that,
174 the as-synthesized QDs-liposome@MB and APTES-coated Fe_3O_4 were added to conjugate the
175 antibody separately and incubated for 1 h at room temperature. The amine group of DSPE-
176 PEG_{2000} phospholipids in the liposome and the APTES of Fe_3O_4 nanoparticles conjugate with
177 the activated carboxylic group of antibodies, and the solution was purified by centrifugation
178 for 10 min at 10,000 rpm to remove the unreacted antibodies and the other coupling agents.
179 The method of sensor preparation and its detection has schematically presented in Fig. S2 of
180 ESM.

181

182 **Optical and electrochemical sensing of CHIK-VP**

183 Antibody-conjugated QDs-liposome@MB and Fe_3O_4 nanoparticles were added with
184 various CHIK-VP concentrations, as mentioned later, and incubated for 10 min to make the

185 sandwich structure. After the antibody-virus binding, an external magnet of 10 mT was placed
186 at the bottom of the mixture solution to remove the detection solutions' impurities and excess
187 reactants. After separating, the detection solution was re-dispersed in a fresh PBS buffer (pH
188 6.8) and transferred in a 96-well microplate. For the disruption of the liposome, 0.1 mM of 5
189 μL chloroform was added in the solution, as mentioned in earlier reports [14], which triggered
190 the liposome's disruption, releasing embedded QDs and encapsulated MB from the liposome.
191 The solution was excited at 400 nm, and the fluorescence intensity was measured in a range of
192 630 – 750 nm before and after the addition of chloroform. Similarly, the solution was separately
193 mixed with the PBS electrolyte. Electrochemical DPV was performed by an SP-150
194 (BioLogic.inc, Tokyo, Japan) in a conventional three-electrode cell consisting of a glassy
195 carbon disk electrode (4 mm in diameter) as working, a Pt wire as counter and a saturated
196 Ag/AgCl, electrode as a reference electrode (EC frontier, Tokyo, Japan) at a fix scan window
197 of −0.4 to 0.0 V.

198

199 ## Results and discussions

200 ### Characterizations of QDs-liposome@MB and Fe_3O_4 nanoparticles

201 To make the precise size of the liposome, the specific composition of phospholipids of DOPC,
202 DOPG, and DSPE-PEG_{2000} amine (50:30:20) were taken according to our previous reports [22].
203 As synthesized, hydrophobic CdSe QDs were used to get embedded in the lipid bilayer of
204 liposome during the film formation step of the lipid. MB was also incorporated while following
205 the hydration step of the liposome so that MB can reside in the inner core of the liposome.
206 After that, 0.2 μm of the polycarbonate membrane was used as a filter to remove the excess
207 MB from the liposome solution. Simultaneously, Fe_3O_4 nanoparticles were synthesized by the
208 sol-gel method, and APTES was coated on it through the standard process of salinization.
209 Initially, these three nanoparticles (QDs, Fe_3O_4, and liposome) were characterized by TEM, as

shown in **Fig. 1**. In **Fig. 1a**, QDs are presented as uniformly dispersed with the range of 5 – 7 nm in size, where the particle distribution shows in **Fig. 1b**. The UV-absorption peak at 650 nm and the fluorescence spectra at 670 nm of the QDs indicate the successful preparation of the CdSe (**Fig. 1c**) [38]. The QDs are dark red under UV light, as shown in **Fig. 1d**. The liposomes are shown in homogeneously distributed spherical form, as presented in the TEM image of **Fig. 1e**. The liposome structures are also characterized by the confocal images where the differential interference contrast (DIC) image (**Fig. 1f**) and fluorescent image (**Fig. 1g**) of liposome displays the completely spherical formation while emitting the strong red fluorescence of QDs in the lipid bilayer. The TEM image of the Fe_3O_4 nanoparticles is shown in **Fig. 1h**. The average diameter of 26.5 nm in a range of 22 – 34 nm of size, as presented in the bar diagram of **Fig. 1i**. Hydrodynamic radii of Fe_3O_4 nanoparticles, QDs-liposome@MB, and QDs-liposome@MB||CHIK-VP||Fe_3O_4 sandwich hybridization nanoconjugates are shown in **Fig. 1j**. The average size of the as-prepared Fe_3O_4 and QDs-liposome@MB are found as 15 and 200 nm, respectively, which resembles the size from their corresponding TEM images. However, after the QDs-liposome@MB||CHIK-VP||Fe_3O_4 sandwich nanoconjugates was formed, the size of the nanoconjugates structure increases near to 900 nm, which indicates the successful construction of the sandwich hybridized structure.

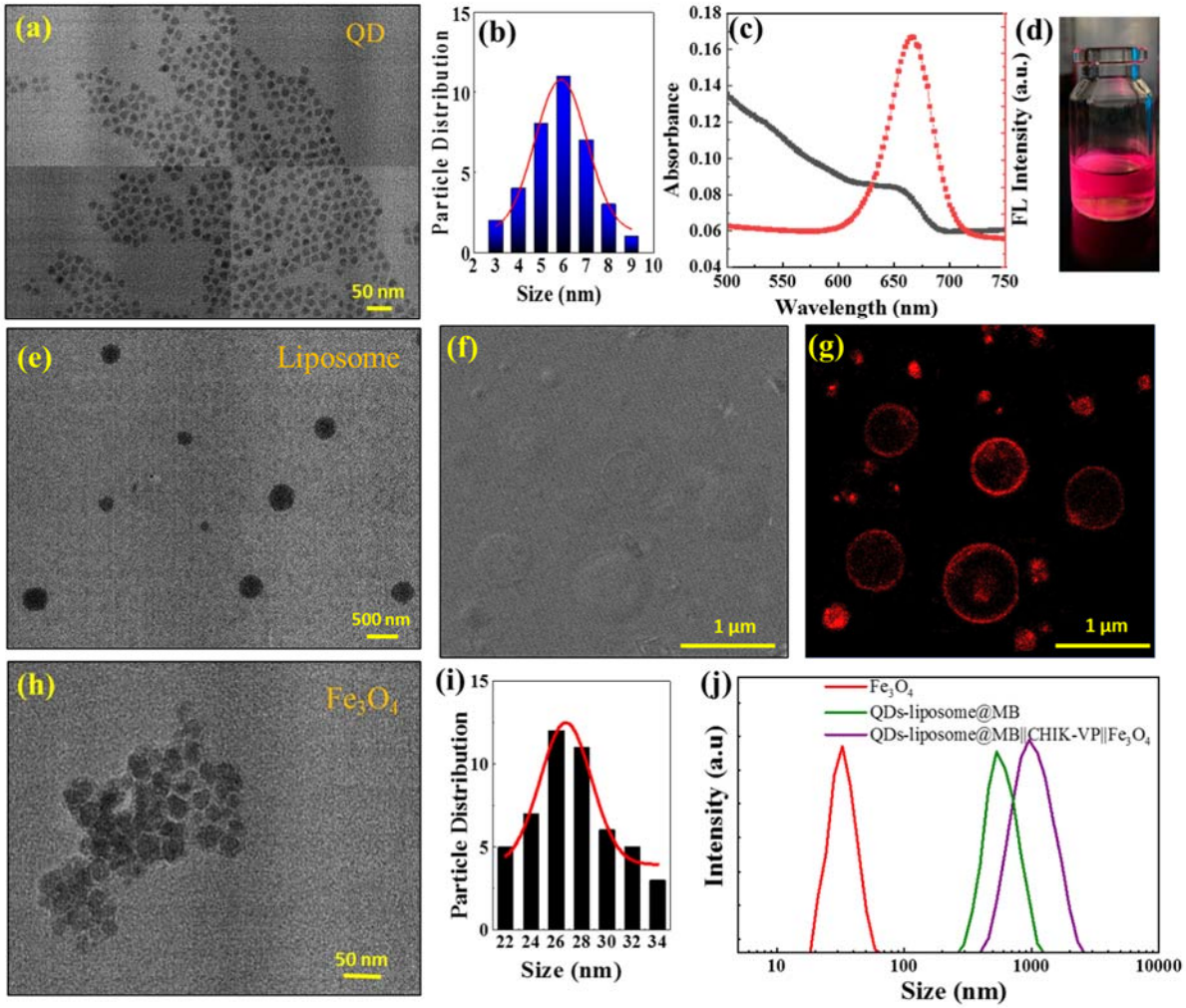

Fig. 1 Characterizations of the as-synthesized CdSe QDs, Fe_3O_4 nanoparticles, and QDs-liposome@MB. (**a**) TEM images, (**b**) particle size distribution, (**c**) UV-Vis absorption and fluorescence emission spectra, and (**d**) fluorescence image under UV light of CdSe QDs. (**e**) TEM images and (**f – g**) confocal images of QDs-liposome@MB. (**h**) TEM image and (**i**) particle distribution of Fe_3O_4 nanoparticles, (**j**) hydrodynamic radius of Fe_3O_4 nanoparticles, QDs-liposome@MB, and QDs-liposome@MB||CHIK-VP||Fe_3O_4 sandwich nanoconjugates.

Formation of QDs-liposome@MB and its optimized condition for virus detection

The as-synthesized QDs-liposome@MB has been initially investigated for the suitable surfactant to release of embedded fluorescent molecules. Among the different surfactants

238 commonly used for the disruption of liposomal formation [39], chloroform shows the best
239 result compared to Triton X and Tween 20 (**Fig. 2a**) [40,41]. In the case of a 1:1 mixture of
240 chloroform and methanol, the liposome's initial perturbation is slightly higher than only
241 chloroform. However, after some time of incubation, the release has been noticed highest in
242 chloroform. As the dissolution of the lipid layer in the chloroform is a slow process, the
243 optimized time for the complete release has been chosen as 10 min, as shown in **Fig. 2b**. After
244 that, the fluorescence enhancement has reached its saturation, confirming the liposome's
245 dissolution time is 10 min. The amount of CdSe QDs has also been optimized with the fixed
246 amount of liposome of 10^3 particles mL^{-1}. Three different concentrations of QDs have been
247 taken to check the optimum condition where the QDs can be entirely embedded in the
248 liposome's hydrophobic surface. In the case of 0.5 and 1 mg mL^{-1} QDs concentration, the
249 fluorescence enhancement is quite satisfactory compared to the low level of 0.1 mg mL^{-1}.
250 However, in the case of 1 mg mL^{-1}, the QDs are not only embedded in the surface but also
251 penetrated inside the liposome, as shown in the inset of **Fig. 2c**. Due to the hydrophobic nature
252 of the QDs, the encapsulated amount of the QDs inside the liposome is completely random and
253 thus should be avoided. Therefore, the moderate concentration of 0.5 mg mL^{-1} of CdSe QDs
254 has been selected for further liposome formation. A similar phenomenon is also observed in
255 the case of DSPE lipid concentration. This amine group-containing lipid has been used in this
256 work to produce the amine functionalization on the surface of the liposome, where the antibody
257 can bind through its carboxylic group [42]. Therefore, it is always good to take the maximum
258 amount of DSPE lipid in the lipid mixture composition without hampering the structure to load
259 the maximum number of antibodies. However, a higher concentration than 1 mM can spill the
260 QDs inside the core. Therefore, to avoid the QDs encapsulation, less than 1 mM of the DSPE
261 lipid has been used (**Fig. 2d**).

262 In the electrochemical sensing, the concentration of the encapsulated redox probe is the
263 most crucial parameter. The maximum concentration of MB can enhance sensitivity. However,
264 the possibility of leakage or the background signal increases with the increasing concentration,
265 resulting in reduced reliability [43]. Therefore, the encapsulation of MB concentration in the
266 liposome was optimized. During the liposome synthesis, three levels of MB concentration (0.1,
267 1, and 5 mM) were used for the MB encapsulation in the core of the liposome and measured
268 different concentrations of CHIK-VP. It is evident from **Fig. 2e**; all different concentrations of
269 MB display excellent linearity in the DPV signal. However, the sensor's blank value in the case
270 of 5 mM concentration is very high, indicating the possible leakage of the MB. Therefore, the
271 highest concentration of 5 mM MB has been rejected. Compared with 0.1 and 1 mM, peak
272 intensities of 1 mM MB is best suited according to their slope of the calibration lines, which is
273 used for remaining studies.

274 Additionally, after optimizing different liposome composition with the concentration of
275 the embedded QDs and encapsulated MB, the construction of the QDs-liposome@MB||CHIK-
276 VP||Fe_3O_4 nanoconjugates were investigated with a different concentration ratio of the Fe_3O_4
277 nanoparticles and QDs-liposome@MB. In this sensing work, the analyte of CHIK-VP bound
278 with antibody-conjugated QDs-liposome@MB and Fe_3O_4 in a sandwich formation and then
279 separated by applying a magnetic step. Therefore, it is obvious that the higher number of
280 magnetic Fe_3O_4 nanoparticles can increase magnetic separation efficiency. However, an excess
281 amount of Fe_3O_4 nanoparticles can bind on the virus surface itself rather than conjugate of the
282 liposome, which may generate a false negative signal. On the other side, the fewer amount of
283 Fe_3O_4 may be unable to bind the virus as well as with the liposomes, producing false-positive
284 signals. Therefore, using the amount of magnetic Fe_3O_4 nanoparticle should be optimized,
285 which is also crucial in this work. A concentration range of 10^{-13} – 10^{-8} g mL^{-1} of CHIK-VP
286 has been applied to the different amounts of magnetic Fe_3O_4 nanoparticles with a fixed

concentration of QDs-liposome@MB. As shown in **Fig. 2f**, the magnetically isolated QDs-liposome@MB||CHIK-VP||Fe_3O_4 nanoconjugates have been tested both fluorometric and DPV method before and after the addition of chloroform. In the case of a low amount of Fe_3O_4, the magnetic nanoconjugates contain a lesser amount of virus particle than the 0.7 mg, which indicates the partial binding of viruses.

On the other hand, a high amount of Fe_3O_4 of 1 and 1.5 mg, though the magnetic adduct successfully separated the viruses. However, it self-quenched the signal due to the MB-Fe_3O_4 and QDs-Fe_3O_4 interactions. Therefore, optimizing all the results, 0.7 mg of Fe_3O_4 nanoparticles proves to be the best-chosen concentration for using in this virus detection system.

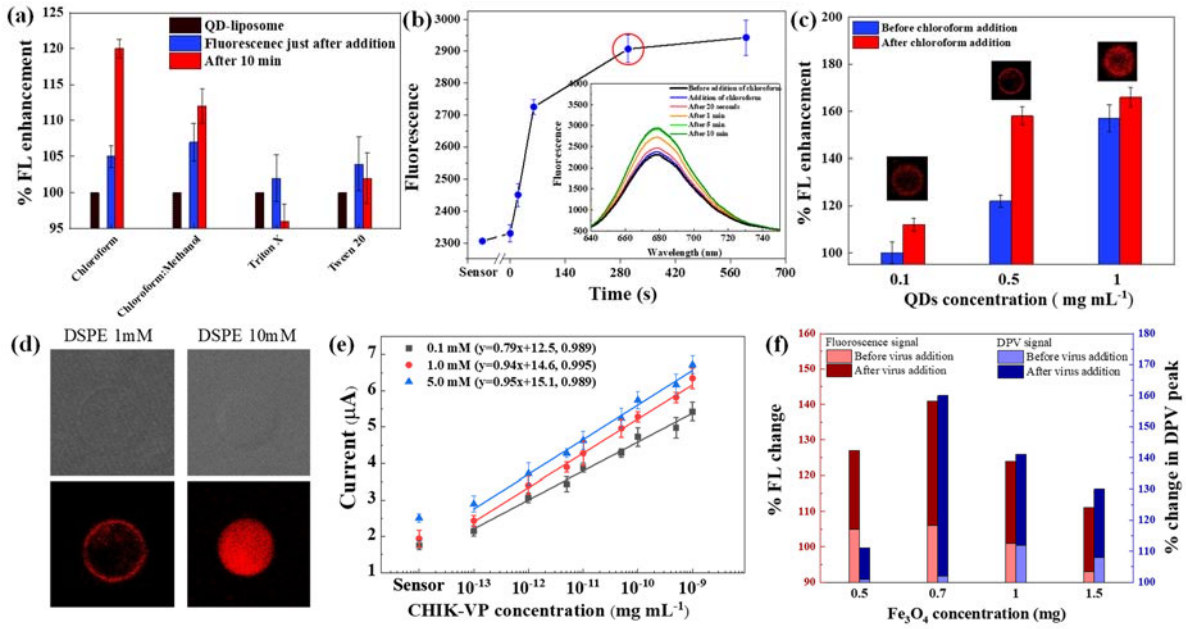

Fig. 2 (**a**) Effect of different surfactants on the disruption of the QDs-liposome@MB, (**b**) time-dependent study on the disruption of the QDs-liposome@MB, (**c**) optimization of the concentration of embedded CdSe QDs in the formation of QDs-liposome@MB, (**d**) confocal images of the QDs-liposome@MB with different concentration of amine-functionalized DSPE lipid, (**e**) optimization of the encapsulated MB, (**f**) optimization of the concentration of Fe_3O_4

302 nanoparticles for the conjugation of the QDs-liposome@MB||CHIK-VP||Fe_3O_4 nanoconjugates
303 in CHIK-VP sensing.

304

305 **Detection of CHIK-VP by QDs-liposome@MB-Fe_3O_4 system**

306 After optimizing all the parameters, the QDs-liposome@MB-Fe_3O_4 system was tested for the
307 applicability for the detection of different concentrations of CHIK-VP. Before the addition of
308 CHIK-VP, there are free antibody-conjugated QDs-liposome@MB and Fe_3O_4 in the reaction
309 medium. However, there is no substantial interaction between these two composites. After
310 adding different concentrations of CHIK-VP and incubating for 10 min, the liposome and
311 nanoparticles were bound with the virus through their corresponding specific antibodies
312 conjugated on the surface of each to make the QDs-liposome@MB||CHIK-VP||Fe_3O_4 sandwich
313 structure. The nanoconjugates were separated magnetically and used to measure the virus
314 concentration by the fluorometric and DPV separately. The fluorometric study was carried out
315 at 400 nm and 672 nm of wavelength for the excitation and emission, respectively, and has
316 shown a strong signal of the QDs after disrupting the liposomes, triggered by chloroform. As
317 shown in **Fig. 3a**, the fluorescence intensities of different CHIK-VP concentrations in the range
318 of 10^{-13} – 10^{-8} g mL^{-1}, evidently indicates the existence of an increasing concentration of
319 released QDs. Before the addition of viruses, the QDs are embedded inside the hydrophobic
320 core of the liposomal wall. Due to the closely packed orientation, the fluorescence of the QDs
321 is not showing any strong peak under excitation. However, after the disruption of the liposome,
322 the free QDs can produce a signal in fluorescence. The calibration line (**Fig. 3b**), based on the
323 intensity of fluorescence, conserves the linearity over the full range of concentration with a
324 correlation coefficient of 0.977. The limit of detection (LOD) has been calculated and obtained
325 from the calibration line, which is 0.56 pg mL^{-1} derived from the $3\sigma/s$ method (three times the
326 standard deviation of the lowest concentration of target/slope of the calibration line) [44]. The

327 TEM **(Fig. 3c)** and confocal images **(Fig. 3d and 3e)** of the nanoconjugates after chloroform
328 addition also corroborate with our hypothesis about the disruption structure of the liposomes.

329 Simultaneously, the QDs-liposome@MB||CHIK-VP||Fe_3O_4 nanoconjugates have also
330 been tested in the electrochemical DPV for the measurement of the released MB. Based on the
331 hypothesis, the addition of chloroform in the liposome mixture, the released MB comes into
332 the buffer. As shown in **Fig. 3f**, the DPV signal of MB at –0.22 V represents CHIK-VP
333 concentration in the concentration range of 10^{-14} – 10^{-8} g mL^{-1}. The calibration line
334 accomplished from the peak current in DPV was calculated and plotted in **Fig. 3g,** which shows
335 the linearity with the correlation coefficient of 0.993. The LOD has been measured from the
336 calibration line of 32.7 fg mL^{-1}, calculated from the 3σ/s method [44] which is one order less
337 than the optical detection due to the high sensitivity of the electrochemical process.

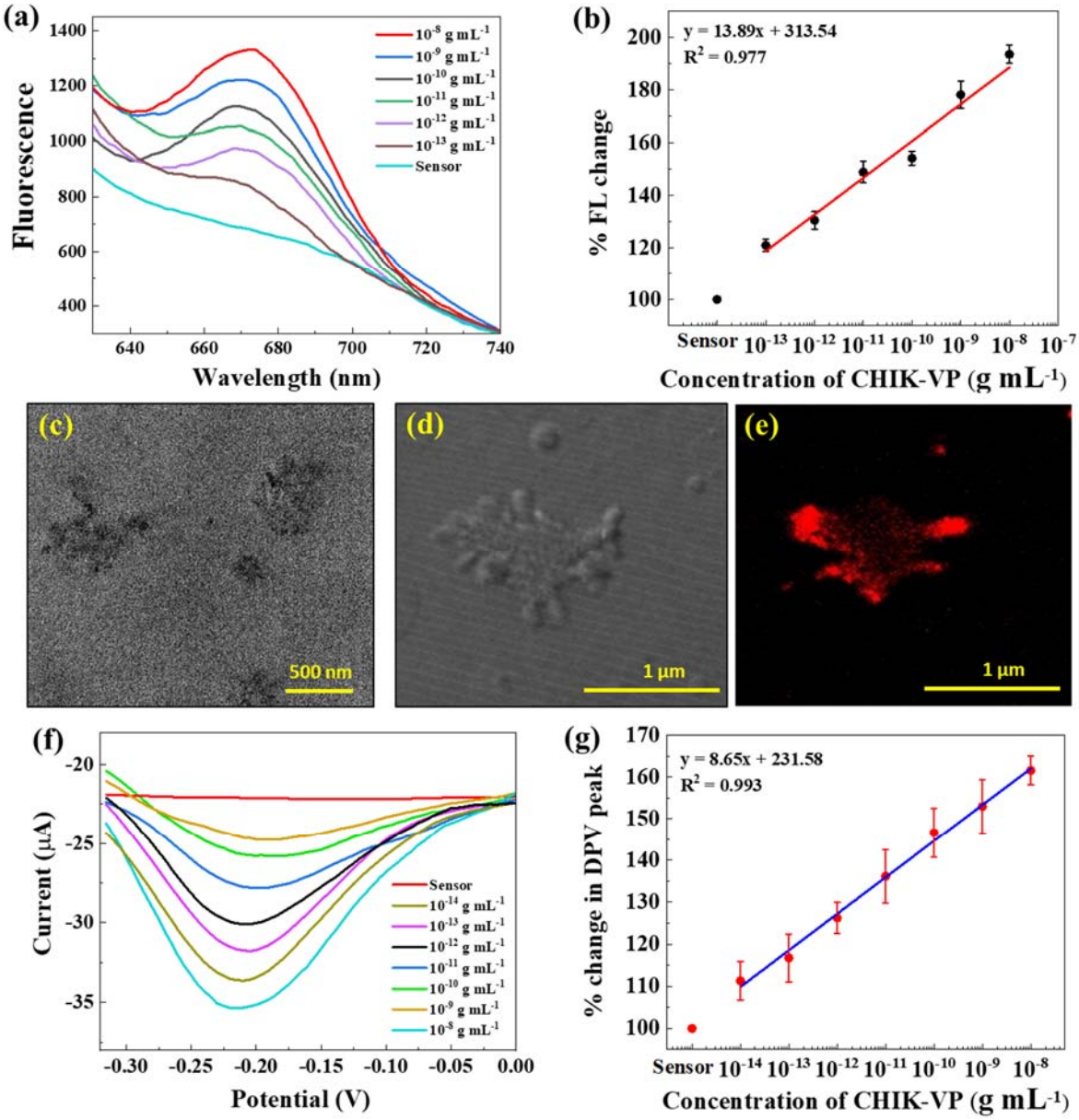

Fig. 3 Detection of CHIK-VP, (a) fluorescence enhancement of CdSe QDs after release from the embedded structure of QDs-liposome@MB||CHIK-VP||Fe_3O_4 nanoconjugates, (b) calibration line in the concentration range of 10^{-13} – 10^{-8} g mL^{-1} of CHIK-VP, (c) TEM image, (d) DIC and (e) fluorescent confocal images of the QDs-liposome@MB||CHIK-VP||Fe_3O_4 nanoconjugates after disruption by chloroform, (f) DPV peak of MB enhancement and its (g) calibration line, after release from the encapsulated structure of QDs-liposome@MB||CHIK-VP||Fe_3O_4 nanoconjugates in the concentration range of 10^{-14} – 10^{-8} g mL^{-1} of CHIK-VP.

346 In comparison with other virus detection methods, as presented in Table 1, the LOD
347 and the range of concentration have clear superiority over other virus detection methods. As
348 CHIK's detection or its protein is rarely reported in the literature, we have compared our results
349 with other methods. In the case of colorimetric and fluorometric sensing, which are the most
350 common detection method due to its simplicity and the possibility for naked-eye detection, the
351 LOD is too poor, not applicable for CHIK diagnosis of this disease. In electrochemical methods,
352 a relatively low LOD has been reported. However, due to the dual approach, the combination
353 of fluorescent and electrochemical, the LOD, and the wide range of concentration range of this
354 current work, is significantly better than others.

355

356 **Table 1** A comparison table for this current method with other virus detection methods in terms
357 of materials, LOD, and detection range.

Detection method	Materials used	Analytes	LOD	Detection range	References
Paper-based Colorimetric	Wax-patterned paper layer, AuNP	NoV	9.5×10^{4} copies mL^{-1}	1.58×10^{5}–7.9×10^{7} copies mL^{-1}	[45]
Fluorometric	AuNP, CdSeTeS QDs	Influenza	3×10^{-10} g mL^{-1}	-	[46]
Fluorometric	Colloidal GNP	Influenza	1.39×10^{-8} g mL^{-1}	5–50×10^{-9} g mL^{-1}	[47]
Fluorometric	QDs, AuNPs	Influenza	9×10^{-7} g mL^{-1}	0.27–12×10^{-9} g mL^{-1}	[48]
Immuno-chromatographic	Colloidal gold	CHIKV (S27/African)	$\geq1\times10^{5}$ PFU mL^{-1}	2.9×10^{-4}–1.6×10^{-8} PFU mL^{-1}	[49]
Electrochemical	ZnO NR, PDMS	Influenza	1×10^{-12} g mL^{-1}	1–10×10^{-9} g mL^{-1}	[49]

Electrochemical	Graphene, AuNP	NoV-LP	100 pM	100 pM–3.5 nM	[50]
Electrochemical	Carbon microarray electrode, AuNP	MERS-CoV	1×10^{-12} g mL^{-1}	$0.01–10000\times10^{-9}$ g mL^{-1}	[51]
Electrochemical	Gold microelectrode	ZIKV protein	10 pM	10 pM–1 nM	[52]
Fluorometric	**QDs-liposome@MB**	**CHIK-VP**	**0.56×10^{-12} g mL^{-1}**	**$10^{-13}–10^{-8}$ g mL^{-1}**	**This work**
Electrochemical			**32.7×10^{-15} g mL^{-1}**	**$10^{-14}–10^{-8}$ g mL^{-1}**	

Selectivity of the sensor

As the antibody conjugation controlled the sandwich structure formation between the target CHIK-VP with QDs-liposome@MB and Fe_3O_4 nanoparticles, it is evident that the sensor should possess high specificity. To confirm its specificity, a selectivity test was performed with other viruses such as WSSV, zika, influenza virus (10^5 copies mL^{-1}), and hepatitis E virus-like particle (10^{-9} g mL^{-1}) and BSA as a negative control. The concentration of all interferences taken for selectivity is higher than their concentrations found in blood, serum, or other sources. The BSA does not show any significant signal in both the detection method of fluorometric and DPV (**Fig. 4**) as expected. Other interfering viruses do not significantly change the signal because the sensing method includes magnetic separation of impurities. A minimal fluorometric response has been observed, which may occur due to the nonspecific interaction with the liposome membrane, which is significantly low compared to the target CHIK-VP's signal. Therefore, from this selective study, it can be noted that the fluorescence and the DPV signal originates only if the specific target virus is present, which confirms its practical

applicability for the virus detection purpose. However, for its real sample analysis, the stability of these materials is a major concern. Due to the formation of the liposomal platform, there is a possibility of leakage of the liposome structure's encapsulated materials over time. In **Fig. S3 of ESM**, the materials' stability shows acceptable results within 2 weeks of its preparation, a disadvantage for its practical analysis. However, the liposomal structure can be replaced by any other stable nanocarrier like solid-lipid nanoparticles or metal-organic frameworks to enhance the stability for the real sample analysis in the future.

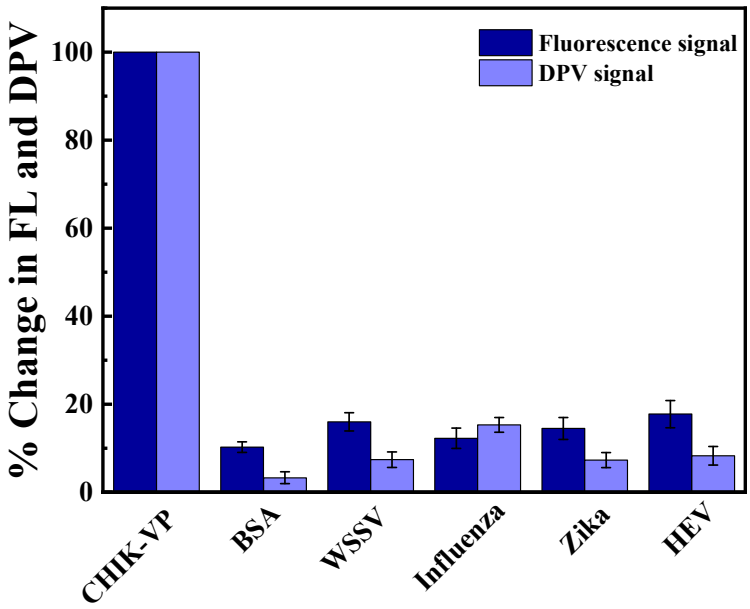

Fig. 4 Selectivity test: fluorometric and DPV signal enhancement of QDs-liposome@MB in the presence of the target CHIK-VP (10^5 copies mL^{-1}), BSA matrix, 10^5 copies mL^{-1} of WSSV, Zika and influenza virus and hepatitis E virus-like particles (10^{-9} g mL^{-1}).

Conclusion

In this work, a liposome-based dual-functional signal amplification system with the combination of magnetic Fe_3O_4 nanoparticles has been developed to detect CHIK-VP. For the

successful blending of these two components, few numbers of virus particles have been able to produce amplified intense signals even in presence of other interferences. A hydrophobic red fluorescent CdSe QDs have embedded and MB solution encapsulated liposome with APTES-coated Fe_3O_4 nanoparticles were prepared separately and conjugated to the anti-CHIK-VP antibody to make specific for the target virus. In presence of various CHIK-VP concentrations, the QDs-liposome@MB and magnetic Fe_3O_4 nanoparticles formed the sandwich-like structured complex which was disrupted for the virus detection purpose. The LOD has been found as 0.56 pg mL^{-1} and 32.7 fg mL^{-1} in fluorometric and DPV process, respectively. Due to the successful fabrication of dual-mode detection probes in a single system, the liposomal matrix could be applied for double responsive sensing for a single analyte. This enhances the reliability of the results exceptionally well, signifying the proposed platform's superiority over other liposome-based systems. Also, the negligible cross-reactivity with other viruses and different matrices, along with low background signals, confirm the specific behavior of the sensor, indicating its potential application in different virus sensing approaches in the near future.

Acknowledgments

Authors thank Professor K. Morita of Institute of Tropical Medicine Nagasaki University, Dr. C. Kawakami of the Yokohama City Institute of Health (Yokohama Japan), Dr. Jun Satoh of National Research Institute of Aquaculture of Japan Fisheries Research and Education Agency, and Dr. Tian-Cheng Li of Department of Virology, National Institute of Infectious Diseases for providing Zika virus, influenza virus A (H3N2), WSSV, and HEV-LP, respectively, for the selectivity test.

Funding

ABG (No. 19F19064) and OJA (No. 19F19348) thank the Japan Society for the Promotion of Science (JSPS) for a postdoctoral fellowship and the Heiwa Nakajima foundation.

Declaration of competing interest

The authors declare no competing financial interest.

References

1. Shojaei TR, Tabatabaei M, Shawky S, Salleh MAM, Bald D (2015) A review on emerging diagnostic assay for viral detection: the case of avian influenza virus. Mol Biol Rep 42 (1):187–199.
2. Luo S-C, Sivashanmugan K, Liao J-D, Yao C-K, Peng H-C (2014) Nanofabricated SERS-active substrates for single-molecule to virus detection in vitro: A review. Biosen Bioelectrons 61:232–240.
3. Vollmer F, Yang L (2012) Review Label-free detection with high-Q microcavities: a review of biosensing mechanisms for integrated devices. Nanophotonics 1 (3–4):267–291.
4. Chowdhury AD, Park EY (2019) Detection of Infectious Viruses using Advanced Nanobiotechnology for Green Society. Green Science and Technology:316–331.
5. Achadu OJ, Kagawa K, Kawahito S, Park EY (2020) Fluoroimmunoassay of influenza virus using sulfur-doped graphitic carbon nitride quantum dots coupled with Ag_2S nanocrystals. Microchim Acta 187 (8):466.
6. Nguyen HH, Park J, Kang S, Kim M (2015) Surface plasmon resonance: a versatile technique for biosensor applications. Sensors 15 (5):10481–10510.

437 7. Kirsch J, Siltanen C, Zhou Q, Revzin A, Simonian A (2013) Biosensor technology: recent
438 advances in threat agent detection and medicine. Chem Soc Rev 42 (22):8733–8768.
439 8. Khoris IM, Chowdhury AD, Li T-C, Suzuki T, Park EY (2020) Advancement of capture
440 immunoassay for real-time monitoring of hepatitis E virus-infected monkey. Anal Chim
441 Acta, 1110: 64–71.
442 9. Ilkhani H, Hughes T, Li J, Zhong CJ, Hepel M (2016) Nanostructured SERS-electrochemical
443 biosensors for testing of anticancer drug interactions with DNA. Biosen Bioelectrons
444 80:257–264
445 10. Stobiecka M, Ratajczak K, Jakiela S (2019) Toward early cancer detection: Focus on
446 biosensing systems and biosensors for an anti-apoptotic protein survivin and survivin
447 mRNA. Biosen Bioelectrons 137:58–71.
448 11. Incani RN, Ferrer E, Hoek D, Ramak R, Roelfsema J, Mughini-Gras L, Kortbeek T, Pinelli
449 E (2017) Diagnosis of intestinal parasites in a rural community of Venezuela: Advantages
450 and disadvantages of using microscopy or RT-PCR. Acta tropica 167:64–70.
451 12. Deng H, Gao Z (2015) Bioanalytical applications of isothermal nucleic acid amplification
452 techniques. Anal Chim Acta 853:30–45.
453 13. Haque F, Li J, Wu H-C, Liang X-J, Guo P (2013) Solid-state and biological nanopore for
454 real-time sensing of single chemical and sequencing of DNA. Nano today 8 (1):56–74.
455 14. Zhou J, Wang Q-x, Zhang C-y (2013) Liposome–quantum dot complexes enable
456 multiplexed detection of attomolar DNAs without target amplification. J Am Chem Soc
457 135 (6):2056–2059.
458 15. Zhao W, Ali MM, Brook MA, Li Y (2008) Rolling circle amplification: applications in
459 nanotechnology and biodetection with functional nucleic acids. Angew Chem Int Ed 47
460 (34):6330–6337.

461 16. Hu J, Zhang C-y (2010) Sensitive detection of nucleic acids with rolling circle amplification
462 and surface-enhanced Raman scattering spectroscopy. Anal Chem 82 (21):8991–8997.
463 17. Ganganboina AB, Chowdhury AD, Khoris IM, Nasrin F, Takemura K, Hara T, Abe F,
464 Suzuki T, Park EY (2020) Dual modality sensor using liposome-based signal amplification
465 technique for ultrasensitive norovirus detection. Biosen Bioelectrons, 157: 112169.
466 18. Chowdhury AD, Park EY (2019) Methylene blue-encapsulated liposomal biosensor for
467 electrochemical detection of sphingomyelinase enzyme. Sens Actuators B 301:127153.
468 19. Johari-Ahar M, Karami P, Ghanei M, Afkhami A, Bagheri H (2018) Development of a
469 molecularly imprinted polymer tailored on disposable screen-printed electrodes for dual
470 detection of EGFR and VEGF using nano-liposomal amplification strategy. Biosen
471 Bioelectrons 107:26–33.
472 20. Chang Y-F, Fu C, Chen Y-T, Jou AF-J, Chen C-C, Chou C, Ho J-aA (2016) Use of
473 liposomal amplifiers in total internal reflection fluorescence fiber-optic biosensors for
474 protein detection. Biosen Bioelectrons 77:1201–1207.
475 21. Das S, Saha P (2018) A review of some advanced sensors used for health diagnosis of civil
476 engineering structures. Measurement 129:68–90.
477 22. Chowdhury AD, Sharmin S, Nasrin F, Yamazaki M, Abe F, Suzuki T, Park EY (2020) Use
478 of Target-Specific Liposome and Magnetic Nanoparticle Conjugation for the Amplified
479 Detection of Norovirus. ACS Appl Bio Mater, 3(6): 3560–3568.
480 23. Hsin T-M, Wu K, Chellappan G (2012) Magnetically immobilized nanoporous giant
481 proteoliposomes as a platform for biosensing. Analyst 137 (1):245–248.
482 24. Harjanto D, Lee J, Kim J-M, Jaworski J (2013) Controlling and assessing the surface
483 display of cell-binding domains on magnetite conjugated fluorescent liposomes. Langmuir
484 29 (25):7949–7956.

485 25. He Y, Li M, Jiang W, Yang W, Lin L, Xu L, Fu F (2016) Phosphatidylserine-functionalized
486 Fe_3O_4@SiO_2 nanoparticles combined with enzyme-encapsulated liposomes for the visual
487 detection of Cu^{2+}. J Mater Chem B 4 (4):752–759.
488 26. Chowdhury AD, Ganganboina AB, Tsai Y-c, Chiu H-c, Doong R-a (2018) Multifunctional
489 GQDs-Concanavalin A@Fe_3O_4 nanocomposites for cancer cells detection and targeted
490 drug delivery. Anal Chim Acta 1027:109–120.
491 27. Dutta Chowdhury A, Agnihotri N, Doong R-a, De A (2017) Label-free and nondestructive
492 separation technique for isolation of targeted DNA from DNA–protein mixture using
493 magnetic Au–Fe3O4 nanoprobes. Anal Chem 89 (22):12244–12251.
494 28. Ganganboina AB, Doong R-A (2019) Graphene quantum dots decorated gold-polyaniline
495 nanowire for impedimetric detection of carcinoembryonic antigen. Sci Rep 9 (1):7214.
496 29. Pastucha M, Farka Z, Lacina K, Mikušová Z, Skládal P (2019) Magnetic nanoparticles for
497 smart electrochemical immunoassays: a review on recent developments. Microchim Acta
498 186 (5):312.
499 30. Yang L, Li N, Wang K, Hai X, Liu J, Dang F (2018) A novel peptide/Fe_3O_4@SiO_2-Au
500 nanocomposite-based fluorescence biosensor for the highly selective and sensitive
501 detection of prostate-specific antigen. Talanta 179:531–537.
502 31. Babamiri B, Hallaj R, Salimi A (2018) Ultrasensitive electrochemiluminescence
503 immunosensor for determination of hepatitis B virus surface antigen using CdTe@CdS-
504 PAMAM dendrimer as luminescent labels and Fe_3O_4 nanoparticles as magnetic beads.
505 Sens Actuators B 254:551–560.
506 32. Nwaji N, Achadu OJ, Nyokong T (2018) Photo-induced resonance energy transfer and
507 nonlinear optical response in ball-type phthalocyanine conjugated to semiconductor and
508 graphene quantum dots. New J Chem 42 (8):6040–6050.

509 33. Ganganboina AB, Chowdhury AD, Doong R-a (2017) Nano assembly of N-doped
510 graphene quantum dots anchored Fe_3O_4/halloysite nanotubes for high performance
511 supercapacitor. Electrochim Acta 245:912–923.
512 34. Yuan P, Southon PD, Liu Z, Green ME, Hook JM, Antill SJ, Kepert CJ (2008)
513 Functionalization of halloysite clay nanotubes by grafting with γ-
514 aminopropyltriethoxysilane. J Phys Chem C 112 (40):15742–15751.
515 35. Nasrin F, Chowdhury AD, Takemura K, Kozaki I, Honda H, Adegoke O, Park EY (2020)
516 Fluorometric virus detection platform using quantum dots-gold nanocomposites
517 optimizing the linker length variation. Anal Chim Acta, 1109: 148-157.
518 36. Pei Z, Anderson H, Myrskog A, Dunér G, Ingemarsson B, Aastrup T (2010) Optimizing
519 immobilization on two-dimensional carboxyl surface: pH dependence of antibody
520 orientation and antigen binding capacity. Anal Biochem 398 (2):161–168.
521 37. Nasrin F, Chowdhury AD, Takemura K, Lee J, Adegoke O, Deo VK, Abe F, Suzuki T,
522 Park EY (2018) Single-step detection of norovirus tuning localized surface plasmon
523 resonance-induced optical signal between gold nanoparticles and quantum dots. Biosen
524 Bioelectrons 122:16–24.
525 38. Maestro LM, Rodríguez EM, Rodríguez FS, la Cruz MI-d, Juarranz A, Naccache R,
526 Vetrone F, Jaque D, Capobianco JA, Solé JG (2010) CdSe quantum dots for two-photon
527 fluorescence thermal imaging. Nano Lett 10 (12):5109–5115.
528 39. Singh S, Vardhan H, Kotla NG, Maddiboyina B, Sharma D, Webster TJ (2016) The role of
529 surfactants in the formulation of elastic liposomal gels containing a synthetic opioid
530 analgesic. International journal of nanomedicine 11:1475.
531 40. Tasi L-M, Liu D-Z, Chen W-Y (2003) Microcalorimetric investigation of the interaction
532 of polysorbate surfactants with unilamellar phosphatidylcholines liposomes. Colloids Surf
533 A 213 (1):7–14.

534 41. Tang Y, Tang D, Zhang J, Tang D (2018) Novel quartz crystal microbalance
535 immunodetection of aflatoxin B1 coupling cargo-encapsulated liposome with indicator-
536 triggered displacement assay. Anal Chim Acta 1031:161–168.
537 42. Vabbilisetty P, Sun X-L (2014) Liposome surface functionalization based on different
538 anchoring lipids via Staudinger ligation. Org Biomol Chem 12 (8):1237–1244.
539 43. Chen D, Wen S, Peng R, Gong Q, Fei J, Fu Z, Weng C, Liu M (2019) A triple signal
540 amplification method for chemiluminescent detection of the cancer marker microRNA-21.
541 Microchim Acta 186 (7):410.
542 44. Dutta Chowdhury A, Doong R-a (2016) Highly sensitive and selective detection of
543 nanomolar ferric ions using dopamine functionalized graphene quantum dots. ACS Appl
544 Mater Interfaces 8 (32):21002–21010.
545 45. Han KN, Choi J-S, Kwon J (2016) Three-dimensional paper-based slip device for one-step
546 point-of-care testing. Sci Rep 6 (1):25710.
547 46. Takemura K, Adegoke O, Takahashi N, Kato T, Li T-C, Kitamoto N, Tanaka T, Suzuki T,
548 Park EY (2017) Versatility of a localized surface plasmon resonance-based gold
549 nanoparticle-alloyed quantum dot nanobiosensor for immunofluorescence detection of
550 viruses. Biosen Bioelectrons 89:998–1005.
551 47. Chang Y-F, Wang S-F, Huang JC, Su L-C, Yao L, Li Y-C, Wu S-C, Chen Y-MA, Hsieh J-
552 P, Chou C (2010) Detection of swine-origin influenza A (H1N1) viruses using a localized
553 surface plasmon coupled fluorescence fiber-optic biosensor. Biosen Bioelectrons 26
554 (3):1068–1073.
555 48. Li X, Lu D, Sheng Z, Chen K, Guo X, Jin M, Han H (2012) A fast and sensitive
556 immunoassay of avian influenza virus based on label-free quantum dot probe and lateral
557 flow test strip. Talanta 100:1–6.

558 49. Okabayashi T, Sasaki T, Masrinoul P, Chantawat N, Yoksan S, Nitatpattana N, Chusri S,
559 Vargas REM, Grandadam M, Brey PT (2015) Detection of chikungunya virus antigen by a
560 novel rapid immunochromatographic test. J Clin Microbiol 53 (2):382–388.
561 50. Chand R, Neethirajan S (2017) Microfluidic platform integrated with graphene-gold nano-
562 composite aptasensor for one-step detection of norovirus. Biosen Bioelectrons 98:47–53.
563 51. Layqah LA, Eissa S (2019) An electrochemical immunosensor for the corona virus
564 associated with the Middle East respiratory syndrome using an array of gold nanoparticle-
565 modified carbon electrodes. Microchim Acta 186 (4):224.
566 52. Kaushik A, Yndart A, Kumar S, Jayant RD, Vashist A, Brown AN, Li C-Z, Nair M (2018)
567 A sensitive electrochemical immunosensor for label-free detection of Zika-virus protein. Sci
568 Rep 8 (1):9700.

569

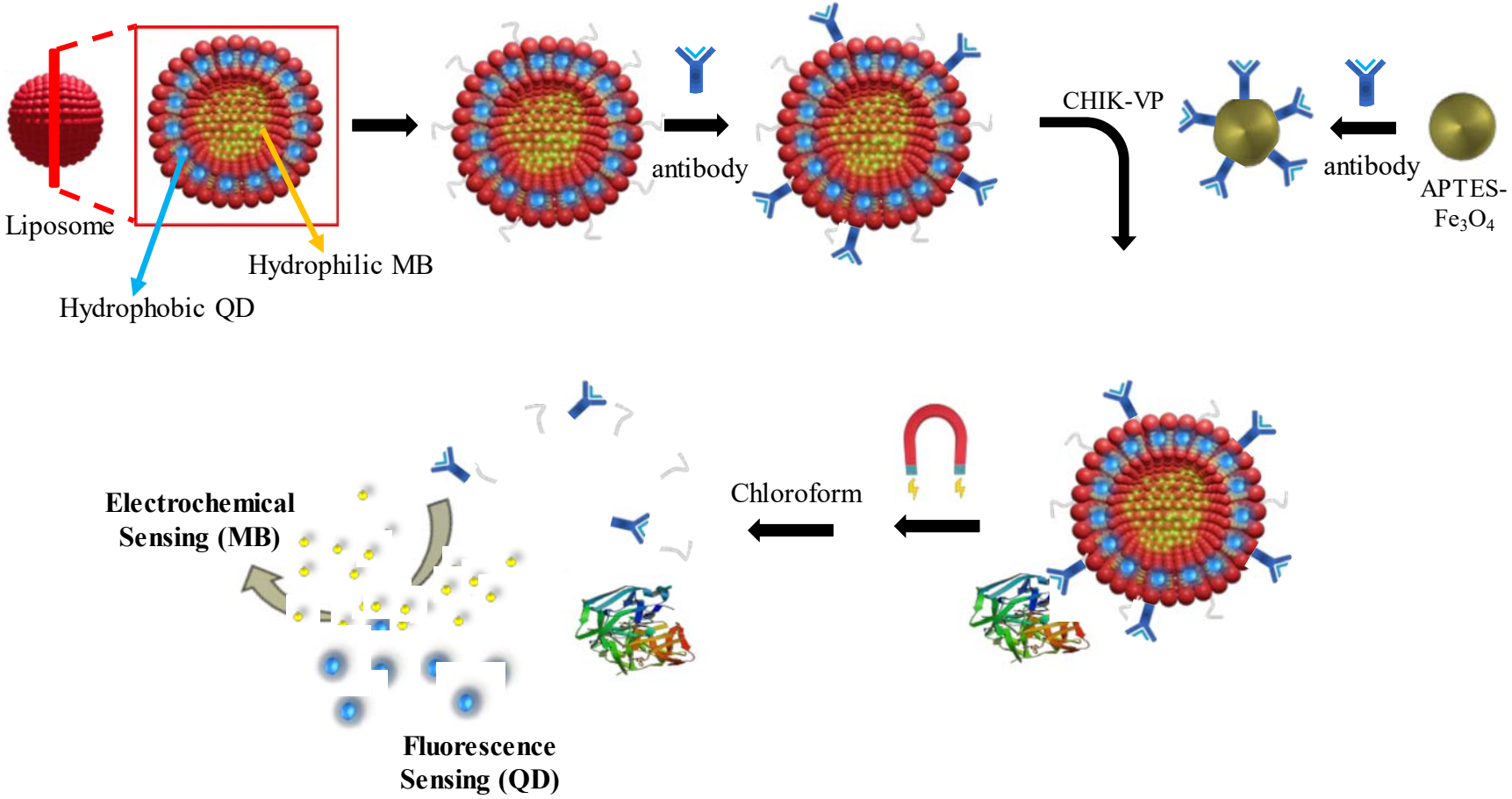
Liposome
Hydrophobic QD
Hydrophilic MB
antibody
CHIK-VP
antibody
APTES-
Fe_3O_4
Chloroform
Electrochemical
Sensing (MB)
Fluorescence
Sensing (QD)

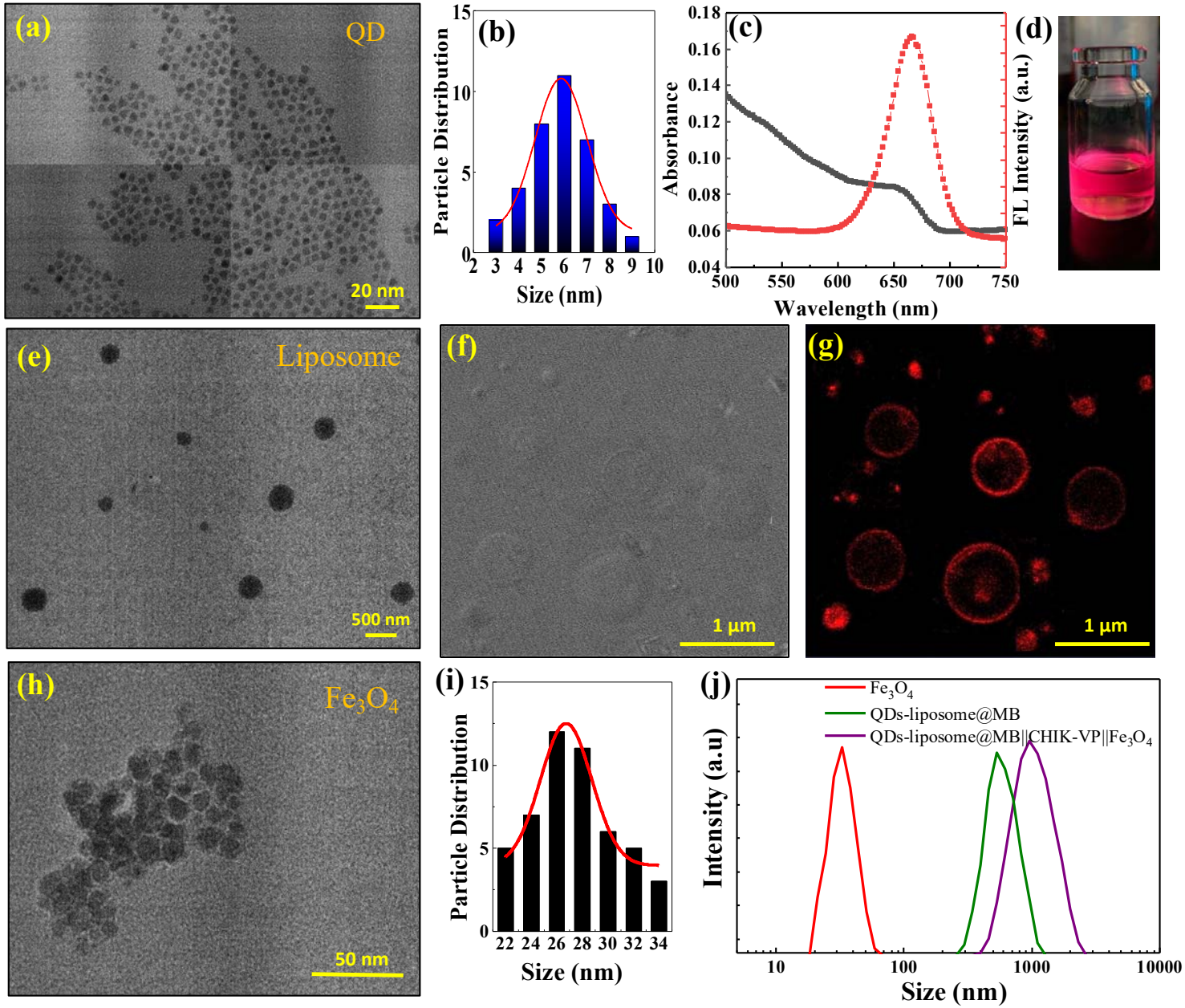
(a)
QD
20 nm
(b)
Particle Distribution
Size (nm)
(c)
Absorbance
FL Intensity (a.u.)
Wavelength (nm)
(d)
(e)
Liposome
500 nm
(f)
1 µm
(g)
1 µm
(h)
Fe3O4
50 nm
(i)
Particle Distribution
Size (nm)
(j)
Fe3O4
QDs-liposome@MB
QDs-liposome@MB||CHIK-VP||Fe3O4
Intensity (a.u)
Size (nm)

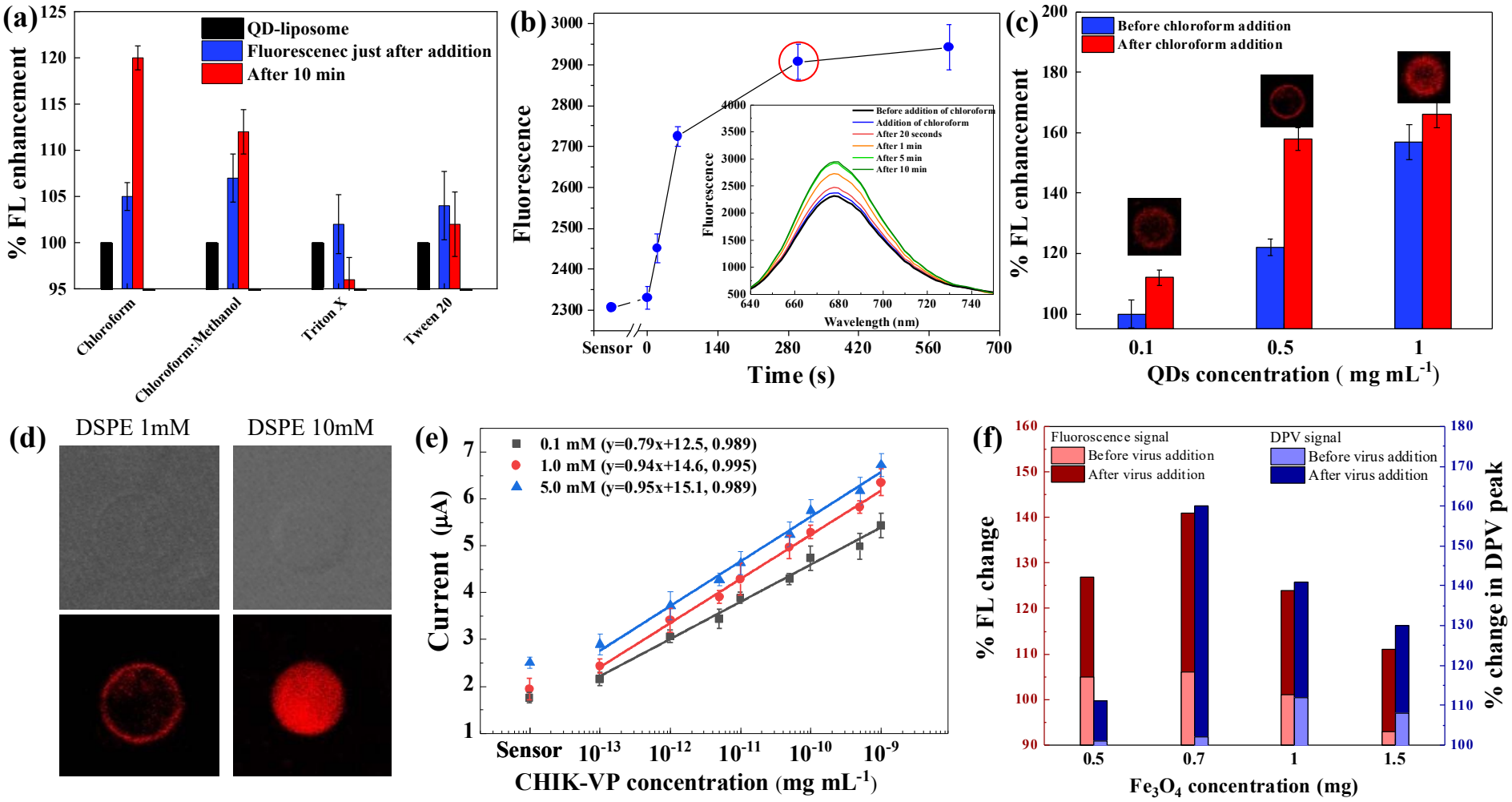
(a)
QD-liposome
Fluorescenec just after addition
After 10 min
% FL enhancement
Chloroform
Chloroform:Methanol
Triton X
Tween 20
(b)
Fluorescence
Time (s)
Sensor
Before addition of chloroform
Addition of chloroform
After 20 seconds
After 1 min
After 5 min
After 10 min
Wavelength (nm)
(c)
Before chloroform addition
After chloroform addition
% FL enhancement
QDs concentration (mg mL-1)
(d)
DSPE 1mM
DSPE 10mM
(e)
0.1 mM (y=0.79x+12.5, 0.989)
1.0 mM (y=0.94x+14.6, 0.995)
5.0 mM (y=0.95x+15.1, 0.989)
Current (μA)
Sensor
CHIK-VP concentration (mg mL-1)
(f)
Fluoroscence signal
Before virus addition
After virus addition
DPV signal
Before virus addition
After virus addition
% FL change
% change in DPV peak
Fe3O4 concentration (mg)

Nasrin et al., Fig. 3

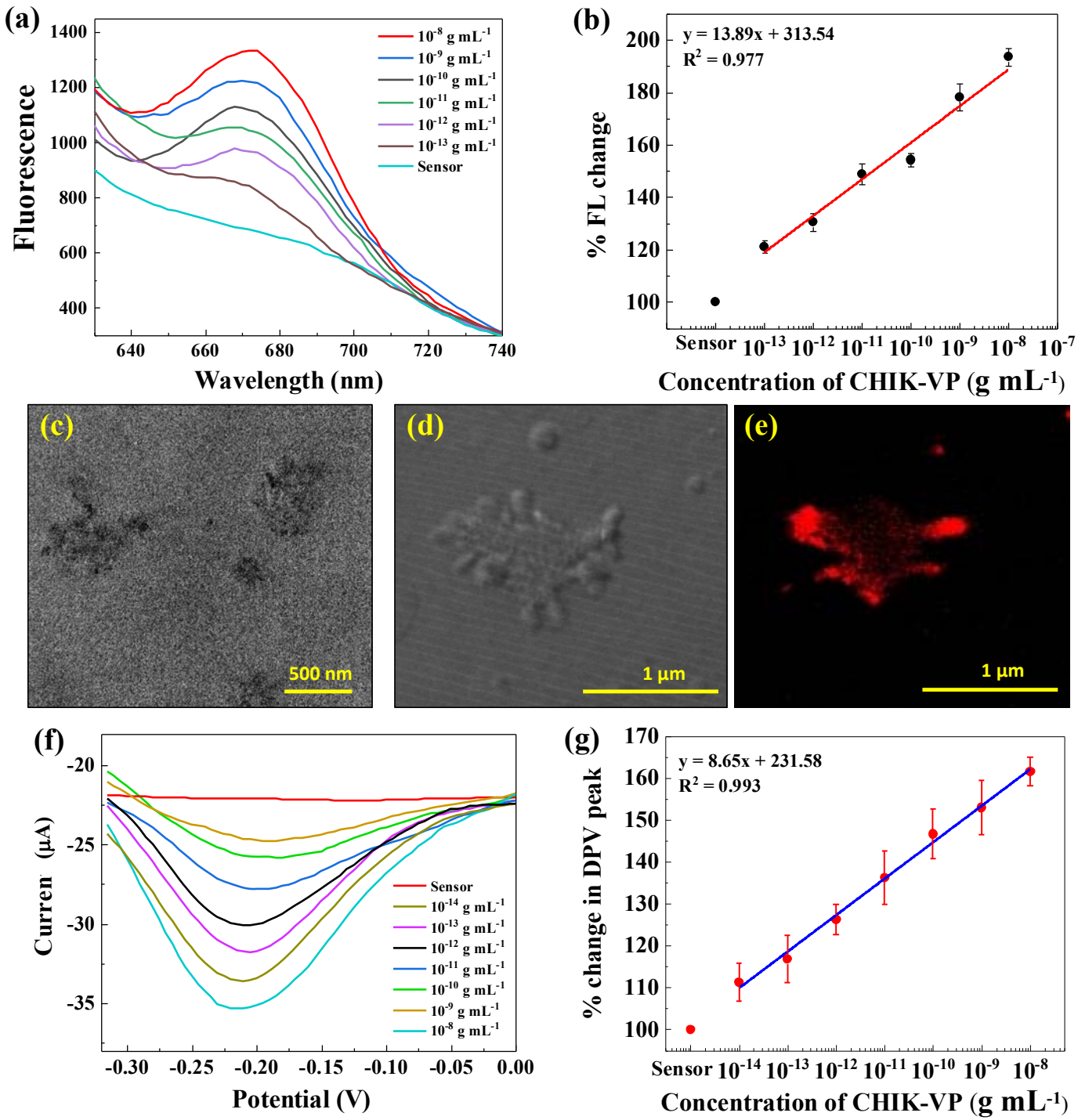

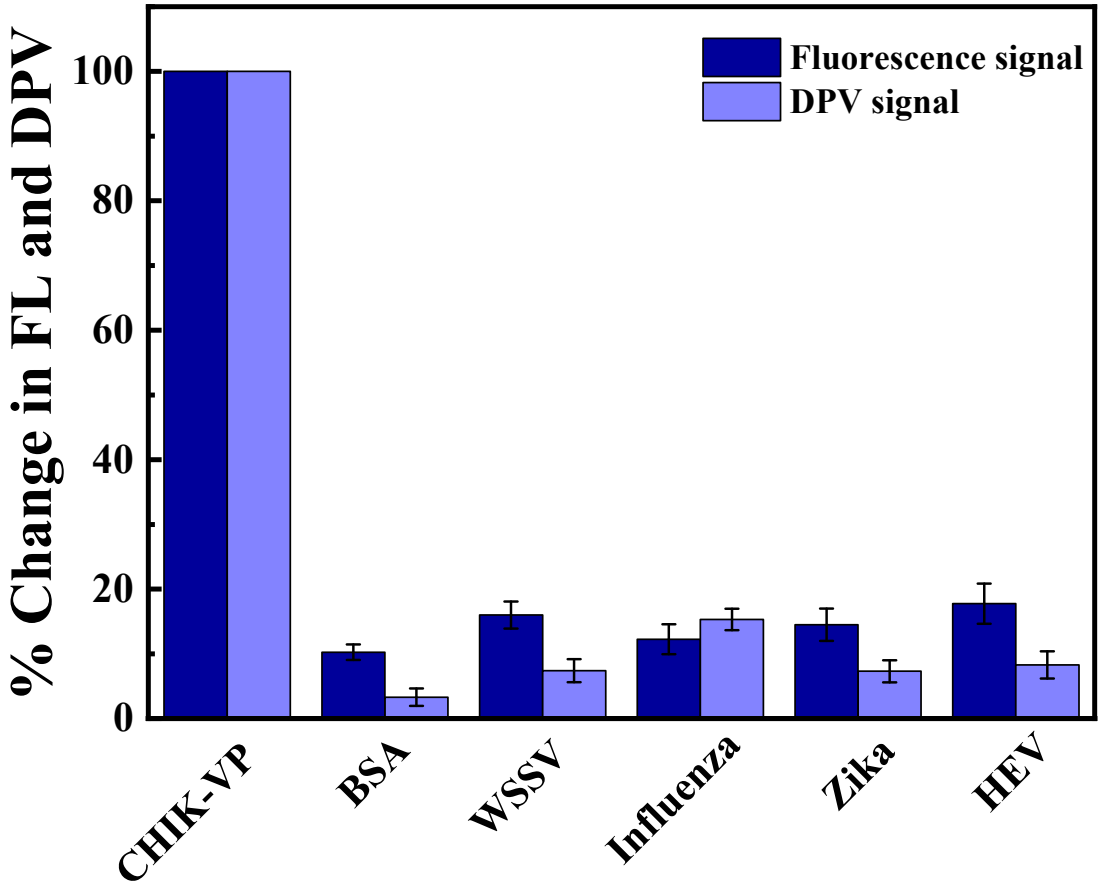
% Change in FL and DPV
100
80
60
40
20
0
Fluorescence signal
DPV signal
CHIK-VP
BSA
WSSV
Influenza
Zika
HEV

Electronic supplementary material

Fluorescent and electrochemical dual-mode detection of Chikungunya virus E1 protein using fluorophore-embedded and redox probe-encapsulated liposomes

Fahmida Nasrin[1,#] · Ankan Dutta Chowdhury[2,#] · Akhilesh Babu Ganganboina[2] · Ojodomo J. Achadu[2] · Farzana Hossain[3] · Masahito Yamazaki[3] · Enoch Y. Park[*,1,2]

[1]Laboratory of Biotechnology, Graduate School of Science and Technology, Shizuoka University, 836 Ohya, Suruga-ku, Shizuoka 422-8529, Japan

[2] Laboratory of Biotechnology, Research Institute of Green Science and Technology, Shizuoka University, 836 Ohya, Suruga-ku, Shizuoka 422-8529, Japan

[3] Research Institute of Electronics, Shizuoka University, 836 Ohya, Suruga-ku, Shizuoka 422-8529, Japan

E-mail
* Enoch Y. Park
park.enoch@shizuoka.ac.jp
Fahmida Nasrin
fahmida.nasrin.17@shizuoka.ac.jp
Ankan Dutta Chowdhury
ankan.dutta.chowdhury@shizuoka.ac.jp
Akhilesh Babu Ganganboina
akhilesh.babu.ganganboina@shizuoka.ac.jp
Ojodomo J. Achadu
ojodomo.john.achadu@shizuoka.ac.jp
Farzana Hossain
farzana.hossain.17@shizuoka.ac.jp (FH)
Masahito Yamazaki
yamazaki.masahito@shizuoka.ac.jp (MY)

[*]Corresponding author at: Research Institute of Green Science and Technology, Shizuoka University, 836 Ohya, Suruga-ku, Shizuoka 422-8529, Japan.
E-mail address: park.enoch@shizuoka.ac.jp (E.Y. Park). Tel (Fax): +81-54-238-4887)

[#]these authors contribute equally

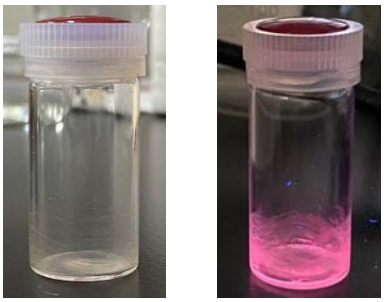

Fig. S1 Lipid film containing QD under normal light and UV light.

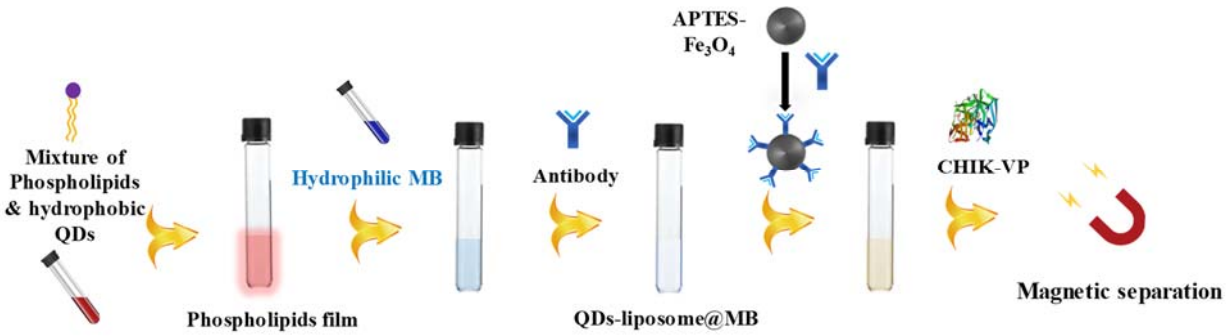

Fig. S2. Experimental steps for the preparation of QDs-liposome@MB and its application towards CHIK-VP detection.

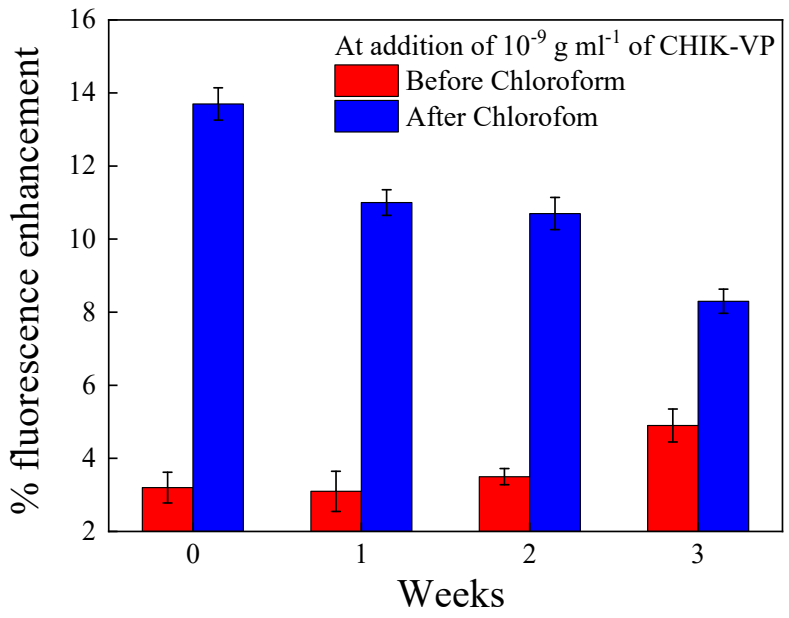

Fig. S3 Stability test of the QDs-liposome@MB nanocomposite over 3 weeks.